Soil Dynamics and Earthquake Engineering 58 (2014) 10–20

Contents lists available at ScienceDirect

Soil Dynamics and Earthquake Engineering

journal homepage: www.elsevier.com/locate/soildyn

In situ tests simulating traffic-load-induced settlement of alluvial silt subsoil

Xinzhuang Cui*, Na Zhang, Jiong Zhang, Zhijun Gao

The Department of Transportation Engineering, School of Civil Engineering, Shandong University, No. 17922, Jingshi Road, Jinan, Shandong Province, PR China

ARTICLE INFO

Article history:
Received 9 November 2012
Received in revised form
26 November 2013
Accepted 28 November 2013

Keywords:
Traffic load
Alluvial silt
Subgrade
Cumulative settlement
In situ tests

ABSTRACT

In China, The Yellow River delta is the youngest large river delta, and the low liquid limit alluvial silt is widely distributed there. The silt is easy to liquefy so that the silt subsoil shows large settlement under traffic load. At present, few in situ model tests were conducted to study the traffic-load-induced settlement of silt subsoil. Therefore, a falling-weight simulation equipment of traffic load was developed. By adjusting the technical parameters such as the falling height of the weight, different types of traffic loads can be well simulated. With the equipment, in situ tests were carried out to study cumulative settlement of silt subsoil in the Yellow River delta. Tests indicate that the settlement and excess pore water pressures rapidly grow initially and then tend to be stable with increasing the number of load cycles, and they also increase with the magnitude of the traffic load. When the load attains a threshold value, liquefaction takes place in the silt subsoil. After terminating loading, the pore water pressure rapidly decreases and the settlement increases simultaneously, while after one hour they tend to stabilize. Based on Chai–Miura cumulative deformation model of soil, the traffic-load-induced cumulative settlement of silt subsoil was calculated and compared with the test results. The calculated cumulative settlement with increasing number of load cycles agrees well with the test results, except the initial phase of cyclic loading where the settlement observed in the situ tests is overestimated. This is mainly because Chai–Miura model assumes undrained conditions while the subsoil under traffic loads is partly drained.

1. Introduction

The Yellow River is China's mother river and the Yellow River delta is a relatively young and large river delta due to frequent river diversion in history. The Yellow River flows through the Loess Plateau and delivers sediment into the Bohai Sea. The sediments deposit at the river mouth and form the Yellow River delta. Alluvial silt is widely distributed in the Yellow River delta and it is newly formed underconsolidated deposit. It has unique characteristics of low liquid limit and plasticity index, small cohesion, low strength, intensive capillarity and poor graduation and water stability, and it is liquefiable soil.

In the near future, a quantity of expressways will be built in the Yellow River delta due to the economic development. In order to occupy less cultivated land and reduce excessive settlement of the underconsolidated subsoil caused by the weight of subgrade, it is necessary to adopt the design method of low road embankment in the Yellow River delta. Note that in this paper, the pavement means the composite structure of surface course, base and subbase, the embankment means the compacted soil layer below the subbase of a road, and the subsoil means the natural soil below a road embankment. The term subgrade includes all layers above natural ground surface. For a road with low embankment constructed on weak subsoil, the traffic-load-induced permanent deformation of the subsoil is one of the important factors which control the design life as well as the maintenance costs of the road. Fujikawa and Miura [1] found that the traffic-load-induced settlement is about 400–600 mm for a low embankment, which is a relatively large settlement in comparison to the allowable settlement for highways. The traffic-load-induced settlement of Chinese Shenzhen–Shantou expressway was found to be about 300 mm though the subsoil was treated with the surcharge preloading method [2]. Large cumulative settlement of subsoil speeds up the destruction of pavement, and leads to great change of transverse slope of pavement and serious ponding on the road. It brings about not only road diseases such as water damage but also traffic safety problems.

Some researchers employed numerical methods like finite element calculations to analyze settlement induced by cyclic load. The development of numerical methods aimed at predicting the behavior of geotechnical structures subject to repeated loading requires the formulation of constitutive models for the constituent soils which are suitable for cyclic loading. Such models may be

* Corresponding author. Tel.: +86 13011744518.
E-mail addresses: cuixz@sdu.edu.cn (X. Cui), znazna@163.com (N. Zhang), jiongzhang@sdu.edu.cn (J. Zhang), 529370405@qq.com (Z. Gao).

0267-7261/$ - see front matter © 2013 Elsevier Ltd. All rights reserved.
http://dx.doi.org/10.1016/j.soildyn.2013.11.010

"implicit" or "explicit". The conventional implicit models are expressed within the framework of elasto-plasticity or hypoplasticity. Explicit (N-type) models directly predict the accumulation of residual strain with increasing number of cycles. For example, relied upon an explicit formulation, a general structure analysis approach was developed by Abdelkrim et al. [3] to predict the traffic-load-induced residual settlement. Niemunis and his coworkers [4] presented a high-cycle explicit model for the accumulation of strain in sand due to small cyclic loading and gave attention to the theoretical aspects of the constitutive description of the cumulative settlement. A large experimental investigation of strain accumulation in granular soils due to long-term cyclic loading is done by Wichtmann [5]. However, using implicit models for the numerical calculations, the number of cycles is usually restricted to a low number. This is due to the large calculation effort on one hand and due to the accumulation of the numerical error on the other hand. The numerical error can become excessive because the number of calculated strain increments is usually large in implicit calculations. Therefore, such implicit models are not suitable for traffic loading. While using explicit models, the number of calculated increments (Delta N) is much lower in numerical calculations, i.e., the numerical error is much less. Furthermore, such models are not restricted with respect to the number of cycles. But the application of sophisticated explicit models may not be justified in the case of simple boundary value problems like a pavement under traffic loading.

A number of empirical models has been proposed to predict the permanent deformation under repeated load. Among them, the power model proposed by Monismith et al. [6] has been widely used. Li and Selig [7] modified the Monismith model based on a large number of laboratory tests, and the dynamic deviatoric stress and static strength of the soil were introduced into the model. Furthermore, Li and Selig [8] showed some successful applications of the modified model to predict the settlement of cohesive soils under train loading. However, the Li–Selig model ignored the effect of the initial static deviatoric stress on the cumulative deformation. Considering the initial static deviatoric stress, Chai and Miura [9] modified the Li–Selig model and applied this model to calculate the permanent settlement of road with a low embankment on soft subsoil. By the multilayer elastic theory, the traffic-load-induced dynamic stress in the subsoil was calculated. Meanwhile, the embankment-load-induced consolidation settlement was simulated by finite element method, and the traffic-load-induced settlement was calculated by the Chai–Miura model. The sum of both types of settlement was compared with the measured data which included deformations of pavement, subbase, subgrade and soft subsoil. The calculated results agreed well with the measured data, although the calculated results were larger at the initial phase and smaller afterwards.

In experimental studies, in the early 1950s, Seed and his coworkers [10,11] studied the settlement behavior of roads under repeated loads by oedometric compression tests. Monismith et al. [6] analyzed the characteristics of permanent deformation of subsoil due to repeated loadings based on cyclic triaxial compression tests. Fujiwara and coworkers [12,13] researched the effect of preloading on the cumulative settlement of clay under cyclic loadings. They concluded that the amount of settlement that occurs after construction depends strongly on the soil overconsolidation ratio, degree of consolidation at the time of unloading, static loading magnitude, and repeated loading magnitude. Yıldırım and Erşan [14] tested cyclic and post-cyclic consolidation settlements of soft clay caused by cyclic loading through undrained cyclic simple shear tests in the laboratory. Shahu et al. [15] studied cumulative plastic strain of a quasi-saturated compacted silty clay under cyclic load by cyclic undrained triaxial tests. Cyclic triaxial tests were also conducted by Liu and Xiao [16] to study the behavior of silt subsoil under various physical states and stress conditions. Though these small-scale specimen tests can evaluate the traffic-load-induced cumulative deformation of subsoil, the results cannot be easily transferred to pavement because the stress and boundary conditions are more complex in real practice.

In order to reflect practical conditions of subsoil in the field, some large-scale physical model tests were carried out. A large-scale bench test was conducted by Bodin-Bourgoin [17] to determine the lateral displacement of ballast. Indraratna [18] carried out a large-scale triaxial test on clay subjected to cyclic loading representing a typical track environment to predict the behavior of soft estuarine subsoil. Huo [19] conducted large-scale model tests to predict the permanent settlement of a composite foundation under cyclic loading. In general, large-scale physical model tests provide reliable results that can reflect the global behavior of cumulative settlement. However, with the limit of the physical model size and inaccurate settings of boundary conditions, the large-scale model tests also cannot perfectly simulate the cumulative settlement occuring in practice.

Therefore, it is necessary to conduct in situ tests for a quantification of the traffic-load-induced settlement of subsoil. In this paper, a simulation equipment of traffic load is described. The design parameters of the equipment are studied to reflect the characteristics of traffic load. With the developed equipment, in situ tests are performed to study traffic-load-induced cumulative settlement of silt subsoil in the Yellow River delta. The in situ test results are compared with numerical calculation results using the model of Chai and Miura.

2. In situ tests

2.1. Description of the site

The test site is located in working section of Xinhe-Xinzhuangzi expressway, as shown in Fig. 1. The subsoil in this area is the low liquid limit silt and geomechanical parameters are shown in Table 1. Groundwater is 0.6 m below the ground surface. Due to intensive capillarity, the average saturation of silt above the groundwater is as much as 0.78. The mean grain size of the subsoil is 0.03 mm. The coefficient of curvature of soil gradation curve is $C_c=d_{30}^2/(d_{60}d_{10})=1.08$, and the coefficient of uniformity is $C_u=d_{60}/d_{10}=3.25$, so the gradation of the soil is poor. A X-ray diffractometer test indicates that non-clay mineral content in the soil is more than 80%.

Electron probe JXA-8800R was employed to analyze the microstructures of silt particles. Fig. 2 shows that the microstructures of test site silt and normal silt particles are obviously different. The normal silt for comparison was piedmont alluvial soil in Jinan with clay removed. Compared with normal silt, the Yellow River delta silt particles were fully rounded with few elongated and flaky particles, and the surface of the particle was crushed and denuded by long time soaking erosion and scouring.

2.2. In situ simulation equipment of traffic load

A falling-weight traffic load simulation equipment (FWTLSE) was developed to measure the cumulative settlement of subsoil. The FWTLSE is mainly composed of three parts: loading system, pneumatic system and automatic control system (Fig. 3). Loading system is made up of loading plate, air spring and supports. The air spring is an inflatable rubber device which takes the place of a steel spring. The stiffness of air spring is changed to simulate the effect of different heights of embankment on the attenuation of wheel-load-induced stress wave. The pneumatic system is

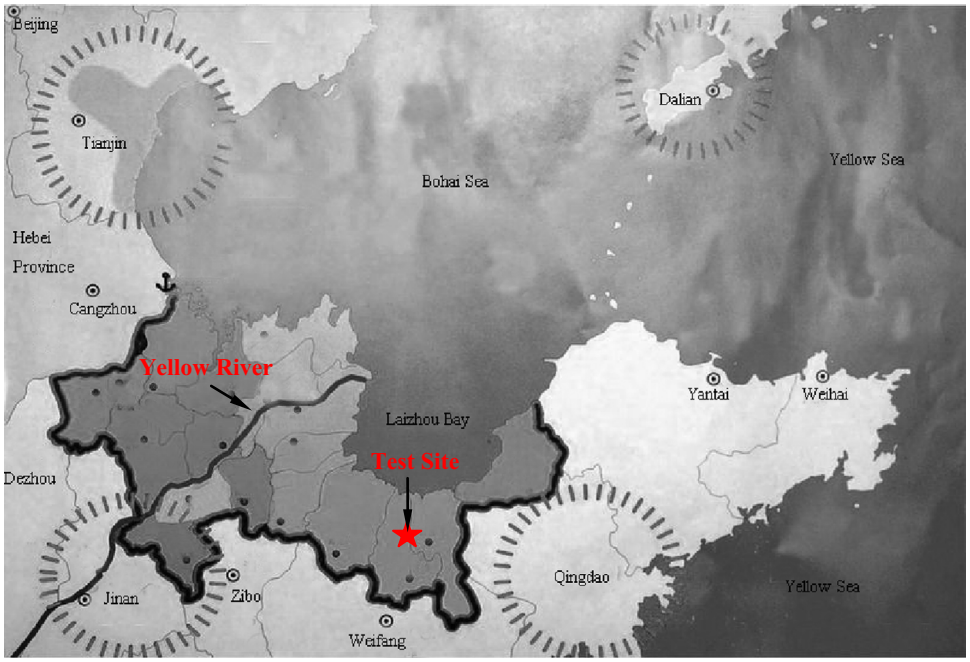

Fig. 1. Location of test site.

Table 1
Geomechanical parameters of subsoil.

Soil layer (m)	Liquid limit (%)	Plastic index (%)	Moisture content (%)	Porosity	Saturation	Effective cohesion (kPa)	Effective friction angle (°)	Compression modulus (MPa)
0–0.6	25	7.4	17.6	0.602	0.78	31.8	22.9	7.45
0.6–10	27	9.8	18.9	0.603	1.00	26.6	20.5	15.86

composed of cylinder, two-position three-way solenoid valve, silencer, stable pressure box and air pump. Air circulation in cylinder is controlled by solenoid valve. Air is compressed into the cylinder by air pump to elevate the falling-weight to a certain height. Then two-position three-way solenoid valve is switched, air in cylinder is squeezed out. The falling-weight falls freely and strikes the air spring on the loading plate. Air is bled through silencer to reduce noise. The automatic control system is made up of single-chip microcomputer (SCM), displacement sensor and computer. Programs of controlling the height of the falling-weight and interval time are written to SCM with computer. When the cylinder is running under the instruction of SCM, displacement sensor connected with cylinder link records the lifting height of the falling-weight, and then the information is fed back to SCM to control the switch of two-position three-way solenoid valve. Then cylinder is operated as preset process. The lifting height of the falling-weight, interval time and the number of loading are displayed on computer screen. The parameters of FWTLSE are adjustable and easy to operate.

2.3. Determination of test target parameters

In order to determine the target parameters range of FWTLSE, the FLAC^{3D} (Fast Lagrangian Analysis of Continua in 3 Dimensions) program was employed to simulate the dynamic response of common highway subgrade under single vehicle load. Simplified wheel load model proposed by Huang [20] was used in the calculation. Contact between tire and road surface is simplified to two circles (Fig. 4). In Fig. 4, δ is 10.65 cm. The load time history of the single wheel load on the road surface can be expressed as

$$\begin{cases} p = p_{max} \sin^2\left(\frac{\pi}{t_0} t\right) & 0 \le t \le t_0 \\ p = 0 & t > t_0 \end{cases} \quad (1)$$

where p_{max} is the load peak and equal to 0.7 MPa which corresponds to the standard axle load of 100 kN according to the specification for design of asphalt pavement in China, and t_0, from 0.01 s to 0.1 s, is the action time of single wheel load and inversely proportional to vehicle speed. When vehicle speed is 120 km/h, t_0 is about 0.03 s.

Pavement structure and material parameters used in the calculation are shown in Table 2. Subsoil is low liquid limit silt and embankment is silty clay. On the basis of the specifications for design of highway subgrades in China, degrees of compaction of embankment soil are 96% (upper layer, 80 cm thick), 94% (middle layer, 70 cm thick) and 93% (lower layer, 0–3 cm thick for the Xinhe-Xinzhuangzi expressway), respectively. The geomechanical parameters of embankment are shown in Table 3.

The vertical stress response curves at the natural ground surface under the center of the wheel gap are shown in Fig. 5. The vertical stress at the ground surface is the superimposed stress of two wheels being part of a wheel group of a truck running on the road. Due to the superposition, the vertical stress under the center of the wheel gap is the largest. It can be seen from Fig. 5 that the height of embankment has a great effect on the vertical stress at the natural subsoil surface. When height of embankment is 0 m, the vertical stress is about 22 kPa. When height of embankment is 0.8 m or 1.5 m, the vertical stress is reduced to 7.8 kPa or 5.6 kPa, respectively. The over loading is very prevalent

on highways in China. Therefore, in order to reflect the effect of overloading and different heights of embankment, the vertical stress amplitudes underneath loading plate of FWTLSE range from 5 kPa to 50 kPa in the test. The thickness of loading plate is 3 mm. This 3 mm thick steel plate has a certain flexibility, therefore, it can simulate the distribution pattern of traffic-load-induced stress attenuated through the subgrade shown as Fig. 6. It can be seen from Fig. 6 that the vertical stress amplitude reduces with the horizontal distance from the center of wheel gap. The falling-weight is the standard penetration test hammer used in engineering geological exploration, with the weight of 63.5 kg, and the diameter of 20 cm. By changing the height of the falling weight

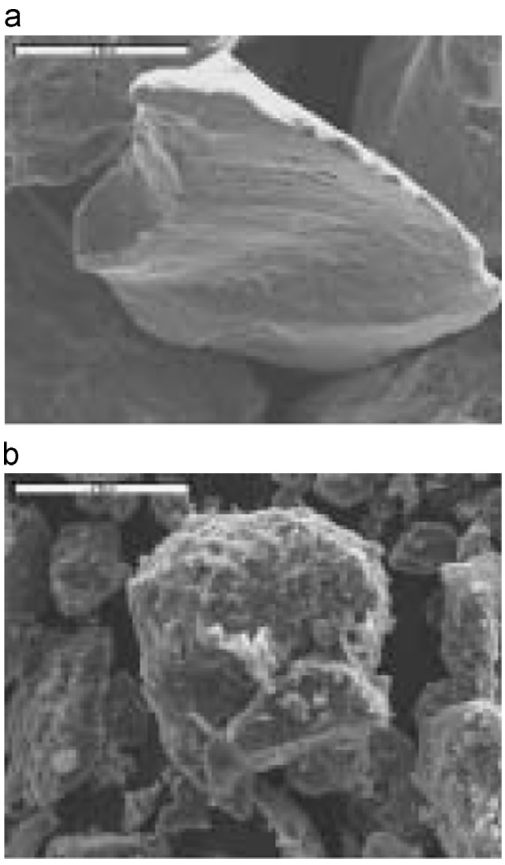

Fig. 2. Microstructure of silt (2 k times): (a) normal silt and (b) silt in the Yellow River delta.

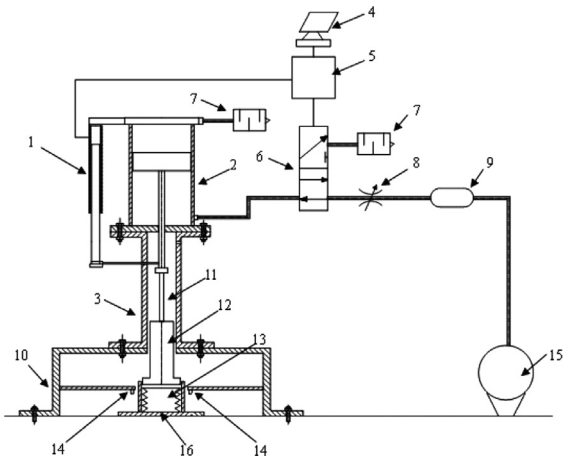

Fig. 3. Schematic overview of in-situ simulation equipment of traffic load. (1) Displacement sensor; (2) Cylinder; (3) Guiding device; (4) Computer; (5) Single chip; (6) Two-position three-way electromagnetic value; (7) Silencer; (8) Throttle value; (9) Stable pressure box; (10) Supports; (11) Lifting rope; (12) Falling weight; (13) Air spacing; (14) Laser displacement meter; (15) Air pump; (16) Loading place.

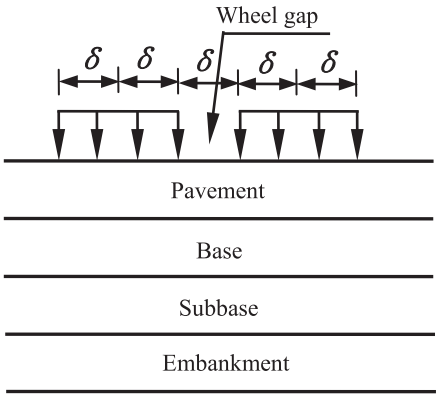

Fig. 4. Model of wheel load distribution on pavement.

Table 2
Elastic parameters of pavement structure and materials.

Layer		Thickness (cm)	Elastic modulus (MPa)	Poisson ratio
Surface course	Upper layer	4	1148	0.25
	Middle layer	6	984	0.25
	Lower layer	8	820	0.25
Base		32	1500	0.3
Subbase		18	750	0.35

Table 3
Geomechanical parameters of embankment.

Soil layer	Degree of compaction (%)	Density (kN/m^3)	Elasticity modulus (MPa)	Poisson's ratio	Cohesion (kPa)	Friction angle (°)
Upper layer	96	20.7	17	0.35	62.5	26.0
Middle layer	94	20.7	13	0.35	20.1	42.4
Lower layer	93	20.7	30	0.35	36.1	35.5

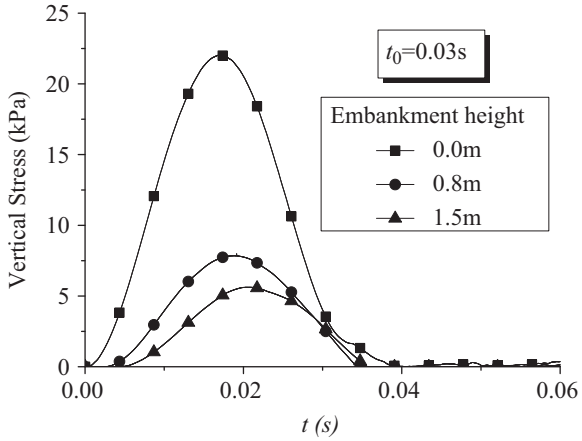

Fig. 5. Time history curves of vertical stresses on subsoil under the center point of wheel gap, obtained from FLAC simulations.

and the stiffness of the air spring, the vertical stress underneath the loading plate is adjusted to meet the desired stress amplitude range.

Fig. 6 shows the vertical stress amplitude curves on natural ground surface varying with the horizontal distance from the center of wheel gap when the height of embankment is 0 m (zero-fill embankment). When the horizontal distance from the center of wheel gap is more than 0.70 m, the vertical stress amplitude changes slowly. In addition, it can be concluded from Fig. 6 that action time of wheel load has little effect on the vertical stress amplitude. In tests, the dimensions of square loading steel plate reflect the range of applied stress. Therefore, the size of the plate can be determined as $1.2 \times 1.2\ m^2$. The radius of its equivalent area circle is 0.68 m which is able to meet test accuracy in the case of zero-fill embankment.

2.4. Arrangement of sensors

Before the in situ tests were conducted, weeds and cover soil on the ground were removed. During and after cyclic loading, some key parameters such as stress, displacement and pore water pressure were measured. The vertical displacement of loading plate was measured with two laser displacement sensors (Fig. 3). The horizontal distances from the center of the loading plate to these sensors were 12 cm. Because the measuring points are located near the center of the loading plate, the mean value of

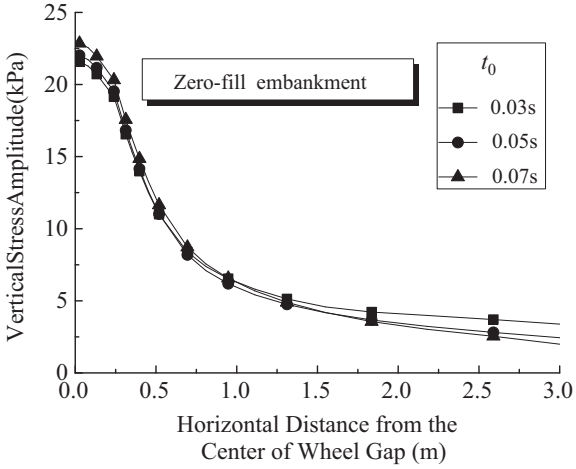

Fig. 6. Curves of vertical stress amplitude on subsoil versus horizontal distance from the center of the wheel gap, obtained from FLAC simulations.

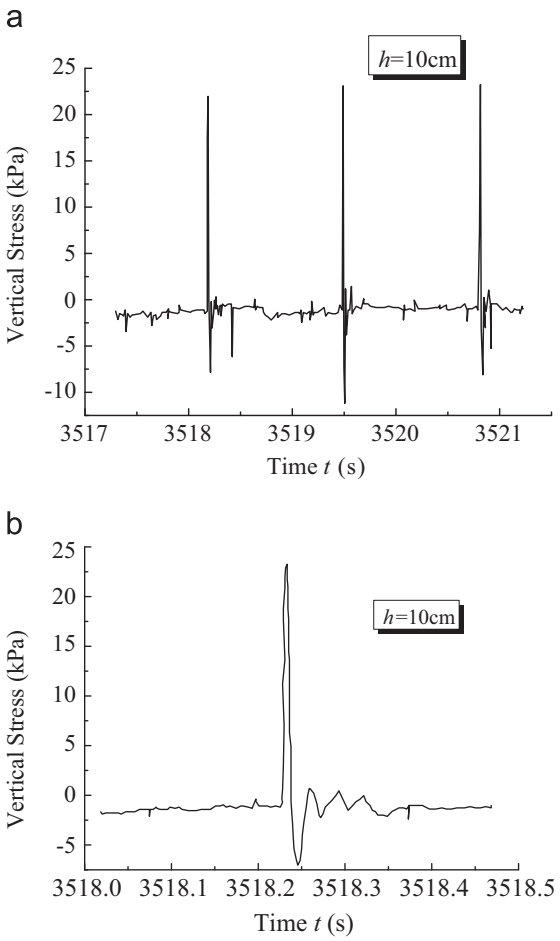

Fig. 8. Measured time history curves of stress on the subsoil under the center point of loading plate: (a) three load cycles and (b) single load cycle.

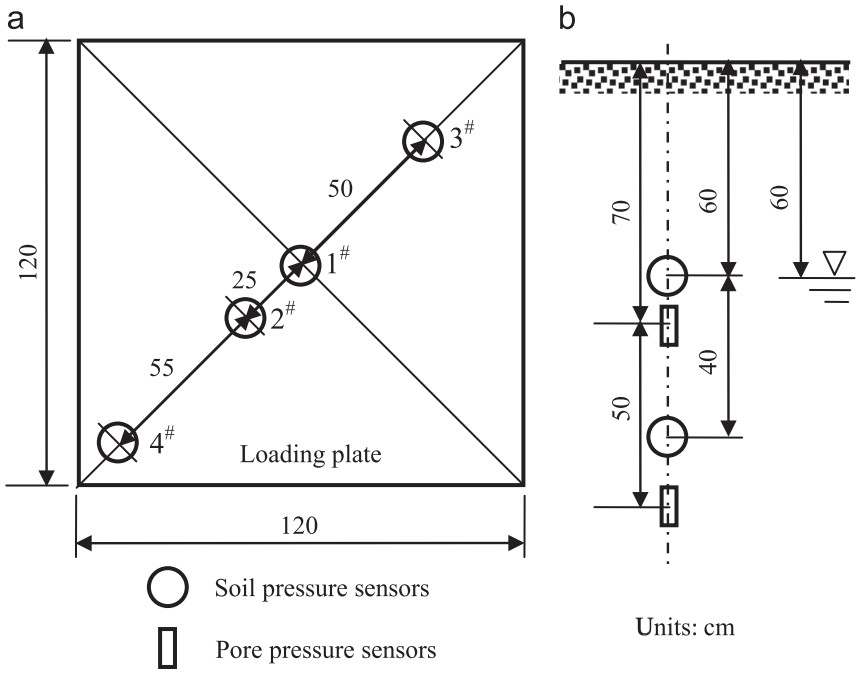

Fig. 7. Positions of sensors.

these two measurements approximately represents the largest displacement of the loading plate. Four dynamic soil pressure sensors were installed at different characteristic positions between loading plate and subsoil surface (Fig. 7(a)). These characteristic positions are basically equidistantly distributed under the loading plate. Two dynamic pore pressure sensors were installed at 0.7 m and 1.2 m underground, respectively, below the center of loading plate. And in the same way, two dynamic soil pressure sensors were installed at 0.6 m and 1.0 m underground, respectively (Fig. 7(b)). All the sensors had been calibrated by the manufacturer and verified by experiments in the laboratory before they were applied in the in situ tests.

2.5. Test results and analysis

2.5.1. Dynamic stress

Within the range from 5 cm to 50 cm, ten different cases of the falling height of the weight were tested every 5 cm. For the case of a falling height $h=10$ cm, the vertical stress response curves measured by the dynamic soil pressure sensor under the center of loading plate are shown in Fig. 8. These signals are basically consistent with the vertical dynamic stress at the surface of natural subsoil caused by a vehicle [21].

The ratio of the peak stress of each sensor on the subsoil surface to the peak stress measured at sensor no. 1 (Fig. 7(a)) is defined as peak stress ratio (*PSR*). Fig. 9 shows the variation of the *PSR* at sensors nos. 2, 3 and 4 with the weight falling height. It can be seen from Fig. 9 that the *PSR* slightly increases with the falling height. The average *PSR* of the sensors nos. 2, 3 and 4 are 0.796, 0.384 and 0.278, respectively (Fig. 10). According to the distribution of *PSR*, the loading plate is divided into four regions, and the representing region of each sensor is shown in Fig. 10. The average *PSR* on subsoil surface underneath the loading plate can be determined from

$$APSR=\frac{\sum PSR_i \times A_i}{L^2} \quad (2)$$

where *APSR*=average peak stress ratio of the loading plate; PSR_i=peak stress ratio of the ith region; A_i=area of the ith region; L=side length of the loading plate. The calculated *APSR* is equal to 0.425, and it is implied that the average peak stress underneath the loading plate is 0.425 times of the peak stress under the center of plate.

Herein the average peak stress is denoted as p_a which is equal to the peak stress measured at sensor no. 1 (Fig. 7(a)) times *APSR*, the dynamic stress period (action time) of single loading as T_0 and the interval time between two loadings as T. Measured variation curves of these parameters with falling height are shown in Fig. 11. When the falling height is smaller than 10 cm, p_a increases strongly with the increase of h. Between 10 and 30 cm p_a varies rather slowly. In the range of 30–50 cm, p_a sharply increases with h again. T_0 nonlinearly decreases with the increase of h. This means that the higher the impacting speed of the falling-weight, the shorter is the dynamic stress duration time. T increases with the increase of h, and this is consistent with real case that the larger the vehicle load, the longer interval time.

The analyses of dynamic stress on the subsoil surface demonstrate that the developed FWTLSE can well simulate the actual wheel-load action. In order to illustrate this, the 10 cm falling distance is taken as an example. The tested stress amplitude below the center of the loading plate is 23 kPa (Fig. 8), whereas for the common type of pavement structure shown in Table 2, the vertical stress peak on the subsoil surface obtained from the numerical calculation is 22 kPa (Fig. 5) when the height of embankment is 0 m and the vehicle speed is 120 km/h. In Fig. 11(b), for the 10 cm falling height, dynamic stress period of single loading is 0.031 s,

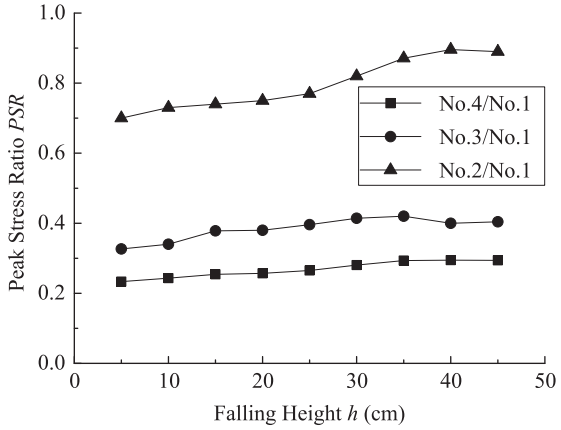

Fig. 9. Variation of peak stress ratio *PSR* with the falling height of the weight measured at sensors nos. 2, 3 and 4.

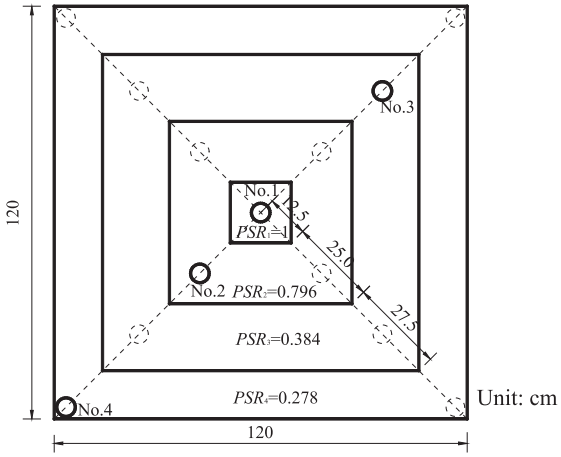

Fig. 10. Assumed distribution of the peak stress ratio below the loading plate.

while in Fig. 5 the calculated one is 0.035 s for zero-filled embankment, that means both values agree well. Therefore, the conclusion can be drawn that the FWTLSE with 10 cm falling height could simulate well the vertical dynamic stress underneath the zero-filled embankment caused by a moving vehicle with the standard axle load and the speed of 120 km/h.

The effect of vehicle overloading can be reflected by increasing the falling height. In Fig. 11(a), the average dynamic stress amplitude for 50 cm falling height is more than three times larger than that for 10 cm falling height. This implies that the developed FWTLSE can simulate a wide range of wheel load.

Fig. 12 shows the variation of vertical dynamic stress peak with depth. The dynamic stress was measured by means of the dynamic soil pressure transducers. It reveals that the vertical stresses attenuate quickly with depth. The greater the falling height, the faster the stress attenuates. For 50 cm falling height, stress peak at 1 m below ground reduces to 20% of that on the subsoil surface.

2.5.2. Excess pore water pressure

Repeated vehicle loads can induce excess pore water pressure in the subsoil, and large excess pore water pressure can cause a liquefaction of the silt subsoil. In test site, the surface layer of subsoil is the 60 cm thick unsaturated hard crust. The in situ tests reveal that some cracks appear on the hard crust surface and mud-pumping occurs as the number of load cycles increases (Fig. 13(a)). This indicates that subsoil had been liquefied. In order to observe the phenomenon of liquefaction inside the subsoil, the cavity

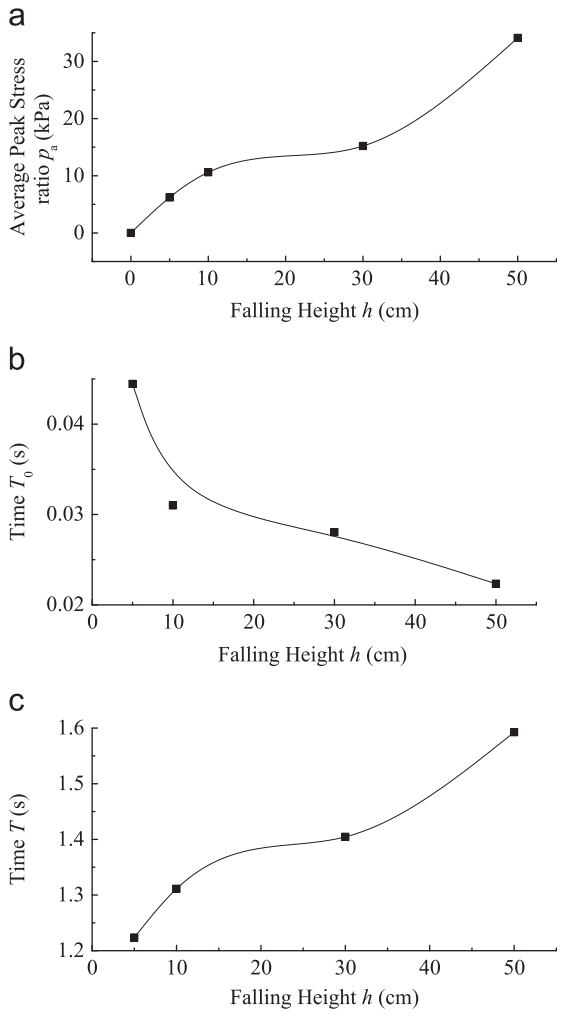

Fig. 11. Variation curves of dynamic stress parameters with falling height of weight: (a) average peak stress; (b) period and (c) interval time.

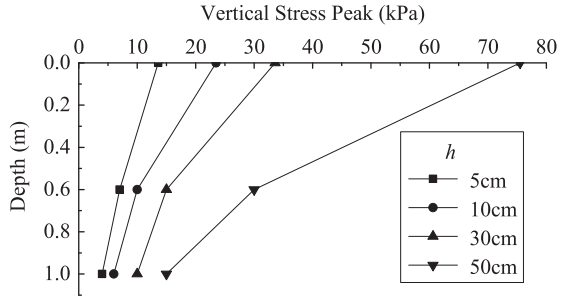

Fig. 12. Variation of vertical stress peak with depth.

shown in Fig. 13(b) was excavated in one of the in situ tests immediately after the cyclic loading. It can be seen that the silt in the bottom of the cavity has become mud. This implies that the original texture of silt has been destroyed due to the cyclic loads.

Excess pore water pressure in subsoil was measured in the process of loading and after terminating loading. Fig. 14 shows the variation of excess pore water pressure at 0.7 m and 1.2 m underground in the process of loading. In most cases, excess pore water pressure linearly increases with the number of load cycles initially, then the rate of pore pressure accumulation gradually gets slower. Yet in some cases, the excess pore water pressure gradually decreases after a certain number of load cycles. The main reason for the differences in the measured curves of excess pore pressure

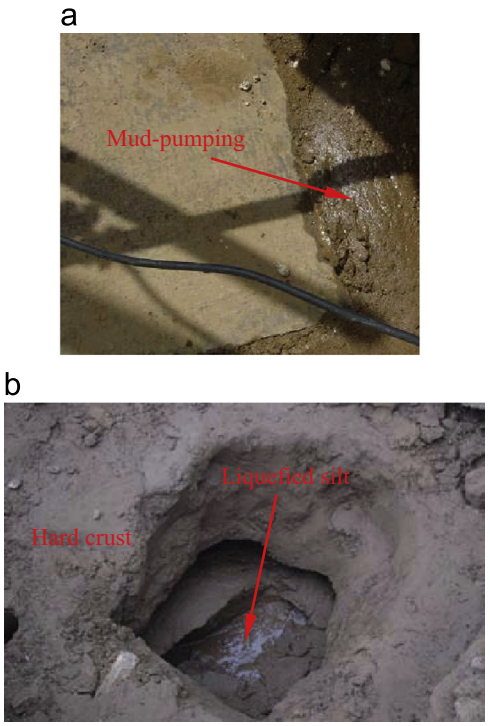

Fig. 13. Liquefaction of silt subsoil: (a) mud-pumping on subsoil surface and (b) liquefaction of silt underneath hard crust.

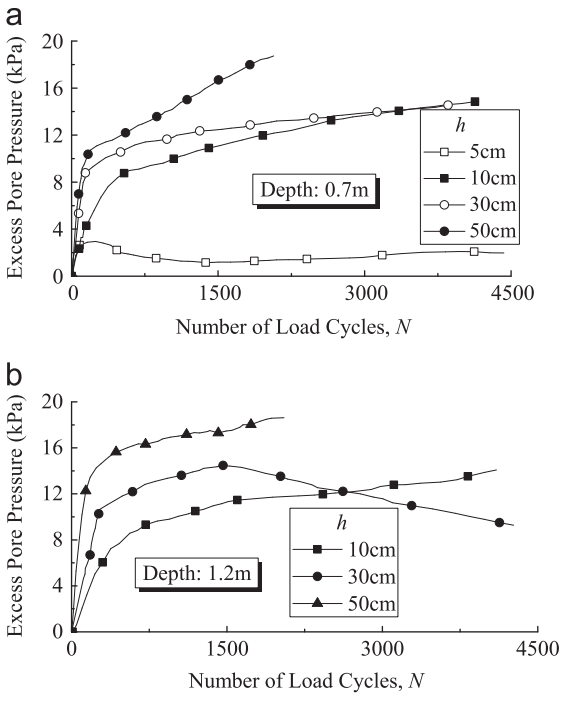

Fig. 14. Development of excess pore water pressure with the number of load cycles in (a) 0.7 m depth and (b) 1.2 m depth.

versus number of cycles is that the development and dissipation of excess pore water pressure in the subsoil occur simultaneously in the process of loading. The spatio-temporal distribution of the excess pore water pressure in the subsoil is complex, and changes of seepage boundary conditions such as the random cracking of hard crust also have an influence on the excess pore water pressure development in the process of loading. In general, the greater the falling distance, the larger the measured excess pore

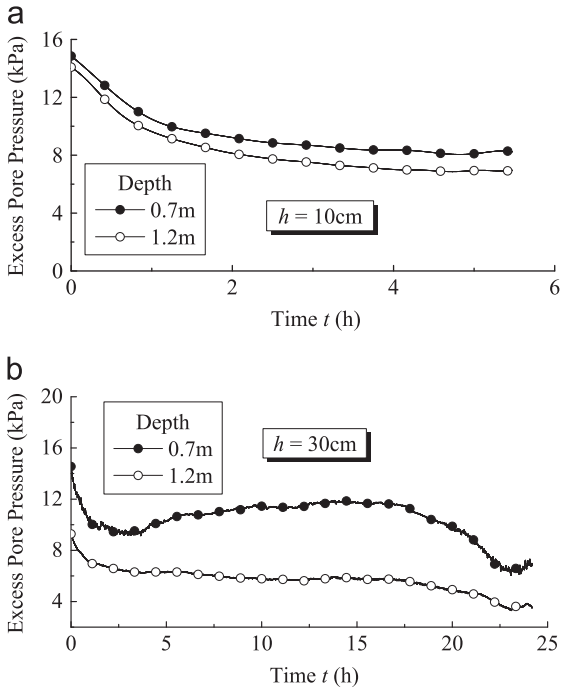

Fig. 15. Development of excess pore water pressure with time after terminating loading for a falling height of (a) $h=10$ cm and (b) $h=30$ cm.

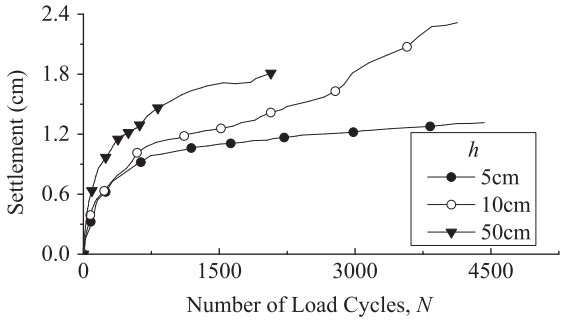

Fig. 16. Development of settlement with the number of load cycles for different falling heights of the weight.

water pressure. Liquefaction takes place only for large amplitudes of the load cycles.

Fig. 15 shows the variations of excess pore water pressure at 0.7 m and 1.2 m underground after terminating loading. In the initial phase (about 1 h), excess pore water pressure is dissipated quickly. Afterwards the speed of dissipation gradually gets slower.

2.5.3. Cumulative settlement

After opening to traffic, the development and dissipation of pore water pressure in the subsoil takes place simultaneously. The dissipation of pore water pressure induces cumulative settlement. In the tests with the FWTLSE the subsoil settlements were measured with the laser displacement sensors in the process of loading and after terminating loading.

Fig. 16 shows the variations of settlement with the number of load cycles in the process of loading. In most cases, the cumulative settlement increases strongly with the number of load cycles at the beginning of cyclic loading, then the rate of settlement accumulation gradually gets slower. The increase of the rate of settlement accumulation at $N>1500$ in the test with $h=10$ cm may be caused by some uncertainties such as the inhomogeneity

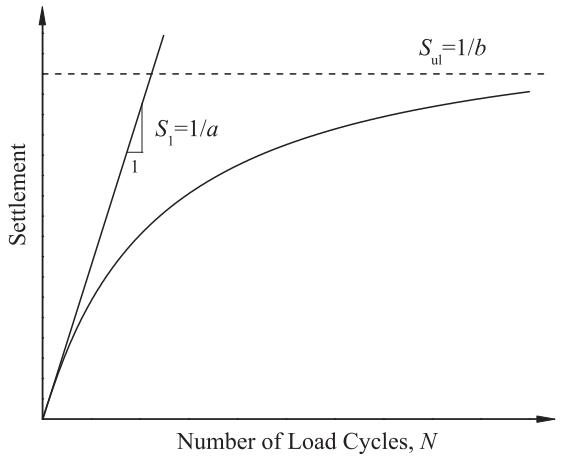

Fig. 17. Variation of the settlement with the number of load cycles.

Table 4
Fitting parameters for different falling heights.

Falling height h (cm)	a (cm^{-1})	b (cm^{-1})	S_1 (cm)	S_{ul} (cm)
5	207.26	0.75	0.0048	1.33
10	175.34	0.69	0.0057	1.45
50	117.19	0.55	0.0085	1.82

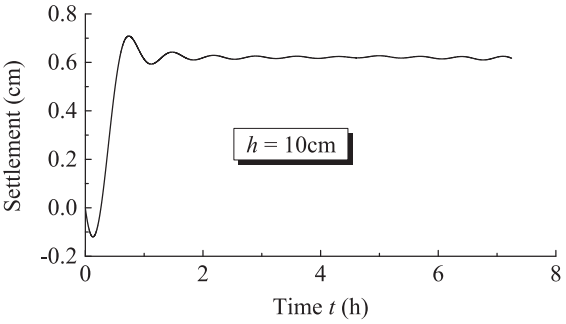

Fig. 18. Development of settlement with time after terminating loading.

of soil. In general, Fig. 16 reveals that the greater the falling distance, the larger is the cumulative settlement.

The variation curves of the settlement with the number of load cycles seem close to the hyperbola, as shown in Fig. 17. So the relationship of the settlement to the number of load cycles can be fitted with the hyperbolic equation as follows:

$$S=\frac{N}{a+bN} \tag{3}$$

where S=settlement; N=number of load cycles; a and b=test parameters determined by the subsoil property.

In Fig. 17, the cumulative settlement generated from the first load cycle S_1 is equal to the reciprocal of a. When N approaches to the infinity, the settlement tends towards the ultimate value S_{ul}, and S_{ul} is equal to the reciprocal of b. For the different falling heights of the weight, the fitting parameters are shown in Table 4. S_1 and S_{ul} increase with the increase of the falling height. The ultimate settlement S_{ul} can be used to evaluate the potential of traffic-load-induced cumulative settlement of subsoil.

Fig. 18 shows the variation of settlement with time after terminating loading in the case of 10 cm falling distance. It can be seen that the characteristic times of the curve shown in Fig. 18 are consistent with those shown in Fig. 18. Within the initial one hour, the settlement and excess pore water pressure both develop

quickly, afterwards they tend to stabilize. This is because the settlement of subsoil after terminating loading is caused by the dissipation of excess pore water pressure.

3. Comparison and discussion

In order to compare with in situ test results, the cumulative settlement of subsoil was numerically simulated using the cumulative deformation model proposed by Chai and Miura [9].

3.1. Chai–Miura cumulative deformation model

Chai and Miura [9] modified empirical models proposed by predecessors to calculate the permanent settlement of roads with a low embankment on soft subsoil. The model considers the effects of initial static deviator stress, the magnitude and the number of traffic load applications and the strength and compression characteristics of the subsoil. The constants in the model are related to physical and mechanical properties of the subsoil, such as the plasticity index and the compression index. The cumulative deformation model can be expressed as follows:

$$\varepsilon_p = a\left(\frac{q_d}{q_f}\right)^m \left(1+\frac{q_s}{q_f}\right)^n N^b \tag{4a}$$

$$q_s = \sqrt{3J_{2s}} \tag{4b}$$

$$q_d = \sqrt{3J_{2d}} \tag{4c}$$

where q_s=initial static deviatoric stress; q_d=traffic-load-induced dynamic deviatoric stress, $q_d = q_{max} - q_s$ with q_{max}=maximum deviatoric stress during the cycles; q_f=static strength of soil; N=number of load cycles; a, b, m and n=constants; J_{2s}=second invariant of initial static stress deviator tensor; J_{2d}=second invariant of dynamic peak stress deviator tensor.

q_f can be determined by the following equation presented by Shen according to the effective consolidation stress theory [22]

$$q_f = c_{cu}\cos\varphi_{cu}/(1-\sin\varphi_{cu}) + \frac{1}{2}(1+K_0)\sigma_{cz}\sin\varphi_{cu}/(1-\sin\varphi_{cu}) \tag{5}$$

where K_0=coefficient of soil pressure at rest; σ_{cz}=overburden pressure; c_{cu} and φ_{cu}=strength parameters of total stress derived from consolidated undrained tests.

Three constants a, b and m are related to the plasticity index of the subsoil. Values suggested for various types of soils by Li and Selig [7] are given in Table 5. The constant n reflects the impact of initial static deviatoric stress on cumulative deformation. Chai and Miura [9] found that the magnitude of cumulative strain linearly increases with initial static deviator stress, so that $n=1.0$ is suggested.

Table 5
Constants of Chai-Miura model suggested by Li and Selig (1996).

Soil type	Parameters		
	a	b	m
CH (high liquid limit clay)	1.2	0.18	2.4
CL (low liquid limit clay)	1.1	0.16	2.0
MH (high liquid limit silt)	0.84	0.13	2.0
ML (low liquid limit silt)	0.64	0.1	1.7

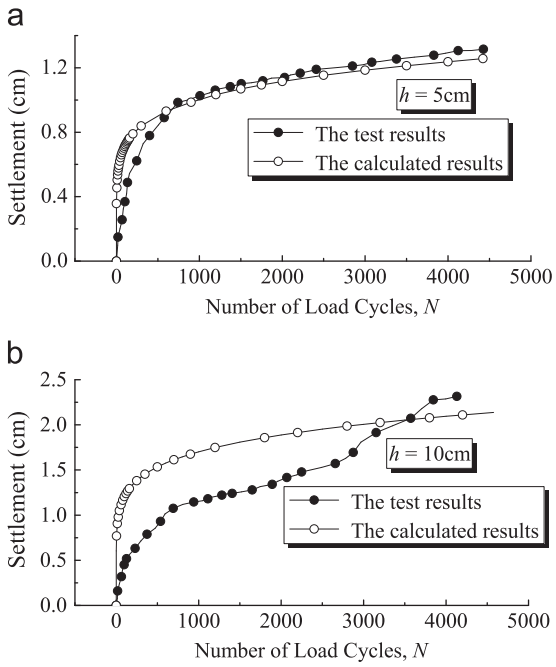

Fig. 19. Comparisons between calculation and test results of cumulative settlement for falling heights (a) h=5 cm and (b) h=10 cm.

3.2. Calculation of cumulative settlement

For simulating the case of in situ test, the cumulative settlement of low liquid limit silt subsoil in the Yellow River delta was calculated and analyzed using the Chai–Miura model. Firstly, the static module of finite difference program Flac^{3D} was used to calculate initial static deviatoric stress q_s in the subsoil due to the own weight of the pavement, embankment and subsoil. Secondly, the dynamic module of Flac^{3D} was employed to simulate the dynamic response of subsoil. In the dynamic calculation, the average vertical dynamic stresses under the loading plate measured in the in situ tests were applied as distributed loads on the subsoil surface to simulate the single wheel loading. Dynamic deviatoric stress q_d can be obtained by the peaks of the dynamic stress in three orthogonal directions. Finally, q_s and q_d were plugged into Eq. (4a), and cumulative deformation of subsoil was calculated. The constants suggested in Table 5 for the ML soil type were used in the calculation (a=0.64, b=0.1 and m=1.7). The static strength of soil q_f was calculated by Eq. (5), with c_{cu} and φ_{cu} values determined from the laboratory tests. For the upper soil layer with depth of less than 0.6 m, c_{cu}=20.0 kPa and φ_{cu}=20.2°, and for the soil below, c_{cu}=14.1 kPa and φ_{cu}=19.0° were applied. The cumulative settlement on the subsoil surface was obtained by integrating the vertical cumulative deformation of soil along depth.

3.3. Comparison and discussion of in situ test and calculation results

Fig. 19 shows the comparisons of cumulative settlement between in situ tests and numerical simulations. It can be seen that the trend of tested cumulative settlement with the number of load cycles is consistent with the calculated results. In general, the calculated settlements develop faster than the measured ones during the early stage of cyclic loading. Especially, when the falling distance is 10 cm, the differences are obvious.

There are several many reasons for the differences between the measured and calculated settlement at the beginning of cyclic loading. The main reason is that the subsoil is partially drained at the site, i.e., the development and dissipation of excess pore water

pressure in the subsoil occur simultaneously in the process of loading. Chai–Miura model used in the numerical simulations, however, has been established based on undrained shear tests. In fact, the spatio-temporal distribution of the traffic-load-induced excess pore water pressure in the subsoil is complex. The development and dissipation of excess pore water pressure is different at different positions in the subsoil. This makes it difficult to simulate cumulative settlement with an empirical model reflecting only undrained conditions. To overcome this deficit, some researchers divided the calculation of cumulative settlement into two steps [23]: First, the settlement caused by undrained shear deformation under traffic load is computed, and second, the consolidation settlement caused by the dissipation of the excess pore water pressure generated in the first step is calculated. The total cumulative settlement is the sum of the settlements obtained from the two steps. A cyclic loading with 1000 cycles and a load period of 1 s is taken as an example. In step one, the pore water pressure accumulation and undrained shear deformation due to the 1000 cycles is calculated. In the second step, the pore pressure dissipation and the accompanying settlement during a time of 1000 s is determined. However, this method also has severe disadvantages. In fact, during the first step, the pore water pressure should be partially dissipated. However, in the two-step method, the whole excess pore water pressure accumulated during the first step is dissipated at once in the second step. The method ignores the nonlinear effect of the simultaneous development of excess pore water pressure and settlement accumulation in the process of cyclic loading.

Another reason probably causing the difference in cumulative settlement between calculation and in situ test is that in the numerical simulation, the parameters a, b and m entering the Chai–Miura model have not been determined experimentally but estimated from Table 5 based on the soil type. In addition, the 60 cm thick unsaturated hard crust at the test site is regarded as a saturated zone in the calculation, and this also causes the calculated settlement to be a little bit larger than measured in the test.

4. Conclusions

In order to study the traffic-load-induced cumulative settlement of the silt subsoil in the Yellow River delta by means of in situ tests, an equipment simulating traffic load was developed. A series of in situ tests were conducted with this equipment. Additionally, for comparison purpose the cumulative settlement was numerically calculated using the Chai–Miura model. The investigation leads to the following conclusions:

(1) The developed simulation equipment can well reproduce the characteristics of traffic load. The large range of design parameters of the equipment can simulate main factors affecting the subsoil settlement such as vehicle overload, the variation of the embankment height and so on. Before performing the in situ test to measure traffic-load-induced cumulative settlement under the action of the standard axle load of 100 kN on the design road, the dynamic stress on the subsoil surface is obtained by numerical calculation. Based on the calculated results, the test target parameters of the simulation equipment are adjusted. With these adjusted parameters, the equipment is applied to measure cumulative settlement of subsoil in situ. The present study performed on Yellow River delta silt found that the traffic-load-induced cumulative settlement in the subsoil grow quickly during the early age of cyclic loading, and then gradually tend to stabilize. The values of ultimate settlement of subsoil can be used to evaluate the potential of traffic-load-induced cumulative settlement of subsoil.

(2) For the tested subsoil, when the amplitude of the load cycles exceeds a threshold value, liquefaction takes place in the silt subsoil. With the increase of wheel load, the cumulative settlement obviously increases. Therefore, restricting vehicle overload is important for reducing cumulative settlement of subgrade.

(3) For the tested subsoil, the cumulative settlements obtained from numerical calculations and those measured in the in situ tests show similar development trends with increasing number of cycles. However, the calculated values are slightly larger at the early stage of traffic loading, due to some assumptions and limitations of the empirical model. For example, undrained conditions are assumed in the calculations with the model while the in situ loading takes place under partly drained conditions. Due to the limitations of the empirical models, in situ tests as proposed in this paper are a meaningful tool for a more accurate prediction of cumulative settlement.

(4) The developed simulation equipment and test method are useful for the practical engineers. At present, there is no final conclusion regarding which height of the embankment should be chosen in order to restrict settlement or prevent liquefaction. The equipment and the test method proposed in this paper can help solving this problem. In the in situ test, if the measured cumulative settlement is out of the range of standard requirements, the height of the falling weight and the stiffness of the air spring will be changed, until the cumulative settlement is acceptable. This adjustment of parameters of the in situ testing equipment can provide the basis for the design of critical embankment height. Furthermore, the equipment and the test method can verify the effectiveness of soil improvement techniques prior to road construction.

Acknowledgments

This work was supported by the Chinese Natural Science Foundations (Nos. 51279094, 51078222 and 50708056), the Independent Innovation Foundation of Shandong University (IIFSDU) (No. 2010JQ001) and the Natural Science Foundations of Shandong Province, China (No. ZR2011EEM012).

References

[1] Fujikawa K, Miura N. Field investigation on the low embankment due to traffic load and its prediction. Soils Found 1996;36(4):147–53.
[2] He GJ. Laboratory test and research on the settlement of soft foundation under low embankment considering the influence of traffic load. Nanjing: Hohai University; 2005 (in Chinese).
[3] Abdelkrim M, Bonnet G, Buhan PD. A computational procedure for predicting the long term residual settlement of a platform induced by repeated traffic loading. Comput Geotech 2003;30(6):463–76.
[4] Niemunis A, Wichtman T, Triantafyllidis TH. A high-cycle accumulation model for sand. Comput Geotech 2005;32(4):245–63.
[5] Wichtmann T. Explicit accumulation model for non-cohesive soils under cyclic loading [Doctoral thesis]. Ruhr University Bochum; 2005.
[6] Monismith CL, Ogawa N, Freeme CR. Cumulative deformation characteristics of subsoil due to repeated loading. Transp Res Rec 1975;537:1–17.
[7] Li D, Selig ET. Cumulative plastic deformation for fine-grained subgrade soils. J Geotech Eng 1996;122(12):1006–13.
[8] Li D, Selig ET. Method for railroad track foundation design. II: Application. J Geotech Geoenviron Eng 1998;124(4):323–9.
[9] Chai JC, Miura N. Traffic-load-induced permanent deformation of road on soft subsoil. J Geotech Geoenviron Eng 2002;128(11):907–16.
[10] Seed HB, Chan CK, Monismith CL. Effects of repeated loading on the strength and deformation of compacted clay. Highw Res Board Proc 1955;34:541–58.
[11] Seed HB, McNeill RL. Soil deformation in normal compression and repeated loading test. Highw Res Board Bull 1956;141:44–53.
[12] Fujiwara H, Ue S, Yasuhara K. Consolidation of alluvial clay under repeated loading. Soils Found 1985;25(3):19–30.

[13] Fujiwara H, Ue S. Effect of preloading on post-construction consolidation settlement of soft clay subjected to repeated loading. Soils Found 1990;30(1):76–86.
[14] Yıldırım H, Erşan H. Settlements under consecutive series of cyclic loading. Soil Dyn Earthq Eng 2007;27:577–85.
[15] Shahu Jt, Yudhbir, Hayashi S. Cumulative plastic strain and threshold stress of a Quasi-saturated compacted silty clay. Lowl Technol Int 2008;10(2):10–20.
[16] Liu JK, Xiao JH. Experimental study on the stability of railroad silt subgrade with increasing train speed. J Geotech Geoenviron Eng 2010;136(6):833–41.
[17] Bodin-Bourgoin V, Tamagny P, Sab K. Experimental determination of a settlement of the ballast portion of railway tracks subjected to lateral charging. Canad Geotech J 2006;43(10):1028–41.
[18] Indraratna B, Rujikiatkamjorn C, Ewers B. Class A prediction of the behavior of soft estuarine soil foundation stabilized by short Vertical drains beneath a rail track. J Geotech Geoenv Eng 2010;136(5):686–96.
[19] Huo TR, Bai SG. Permanent settlement prediction of composite foundation improve by cement–soil piles under cycle loading. Adv Mater Res 2012;482–484:1205–8.
[20] Huang YH. Pavement analysis and design. Delhi: Pearson Education; 1993.
[21] Lu Z, Yao HL, Wu WP, Cheng P. Dynamic stress and deformation of a layered road structure under vehicle traffic loads: experimental measurements and numerical calculations. Soil Dyn Earchq Eng 2012;39:100–12.
[22] Shen ZJ. Earth pressure of clay based on effective consolidation stress theory. Chin J Geotech Eng 2000;22(3):353–6 (in Chinese).
[23] Cui XZ. Traffic-load-induced cumulative settlement of soft clay subgrade of low road embankment. Chin J Highw Transp 2009;22(4):1–8 (in Chinese).